REPORT DOCUMENTATION PAGE

Form Approved OMB No. 0704-0188

1. REPORT DATE *(DD-MM-YYYY)*	2. REPORT TYPE	3. DATES COVERED *(From - To)*
	Paper	

4. TITLE AND SUBTITLE

5a. CONTRACT NUMBER

5b. GRANT NUMBER

5c. PROGRAM ELEMENT NUMBER

6. AUTHOR(S)

5d. PROJECT NUMBER

5e. TASK NUMBER

5f. WORK UNIT NUMBER

7. PERFORMING ORGANIZATION NAME(S) AND ADDRESS(ES)

Air Force Research Laboratory (AFMC)
AFRL/PRSP
5 Pollux Drive
Edwards AFB CA 93524-7048

8. PERFORMING ORGANIZATION REPORT

9. SPONSORING / MONITORING AGENCY NAME(S) AND ADDRESS(ES)

Air Force Research Laboratory (AFMC)
AFRL/PRS
5 Pollux Drive
Edwards AFB CA 93524-7048

10. SPONSOR/MONITOR'S ACRONYM(S)

11. SPONSOR/MONITOR'S NUMBER(S)

12. DISTRIBUTION / AVAILABILITY STATEMENT

Approved for public release; distribution unlimited.

MEMORANDUM FOR PRS (In-House/Contractor Publication)

FROM: PROI (STINFO) 03 July 2002

SUBJECT: Authorization for Release of Technical Information, Control Number: AFRL-PR-ED-TP-2002-176
Erik Antonsen (U. of Illinois) et al., "Herriott Cell Augmentation of a Quadrature Heterodyne Interferometer"

55907 Spanjers

Review of Scientific Instruments
(Deadline: 31 July 2002)

(Statement A)

15. SUBJECT TERMS

16. SECURITY CLASSIFICATION OF:			17. LIMITATION OF ABSTRACT	18. NUMBER OF PAGES	19a. NAME OF RESPONSIBLE PERSON
					Leilani Richardson
a. REPORT	b. ABSTRACT	c. THIS PAGE	A		19b. TELEPHONE NUMBER *(include area code)*
Unclassified	Unclassified	Unclassified			(661) 275-5015

7 items enclosed

Submitted to Review of Scientific Instruments

Herriott Cell Augmentation of a Quadrature Heterodyne Interferometer

Erik L. Antonsen and Rodney L. Burton
University of Illinois at Urbana-Champaign, IL 61801

Gregory G. Spanjers and Scott F. Engelman
Air Force Research Laboratory, Propulsion Directorate, Edwards AFB, CA 93524

ABSTRACT

A quadrature heterodyne interferometer is augmented with a Herriott Cell multi-pass reflector to increase instrument resolution and enable a separation of the phase shift due to neutral density from room vibrations. In addition, the use of the Herriott Cell enables variations in the multi-pass laser-beam geometry that optimizes the diagnostic for small scale length measurements or for planar measurements. Ray tracing analysis is used to illustrate retro-reflective planar measurement geometries attainable with the instrument. Analysis is performed to show that phase front degradation and loss of scene beam intensity, concomitant with the large number of reflections from the Herriott Cell mirrors, does not introduce a systematic measurement uncertainty. The diagnostic capability is demonstrated with measurements of the electron and neutral densities in the plasma exhaust from electric propulsion thrusters. Experimental data with up to 18 passes through plasma demonstrates that the instrument resolution to electron and neutral density increases almost linearly with number of passes. However, measurement uncertainty associated with room vibrations is shown to remain constant as the number of passes is increased. Therefore the Herriott Cell can be used to increase the signal of neutral density phase shifts relative to the noise of the phase shifts due to room vibrations. For the Pulsed Plasma Thruster plasma exhaust used to validate the instrument, the addition of the Herriott Cell reduces the density measurement uncertainty to equal or less than the uncertainty due to discharge irreproducibility. When used on plasma sources with higher reproducibility, the Herriott Cell interferometer should be an effective tool for high resolution electron and neutral density measurements.

1. INTRODUCTION

Plasma and neutral density measurements are critical in the development of the Pulsed Plasma Thruster (PPT).[1] A PPT is a spacecraft propulsion device that uses a pulsed (~10 μs) electrical surface discharge across the face of a solid Teflon™ propellant. The discharge ablates a small amount of material (~3 μg), ionizes it to plasma, and electromagnetically accelerates it to create thrust. Following the pulsed discharge a larger mass (~25 μg) of neutral vapor is emitted from the device on a much longer time scale (~1 ms). The electron and neutral density measurements are needed to better understand the conversion from solid Teflon™ propellant to plasma accelerant. In addition, exit plane density measurements are needed to develop and verify models of interaction between the spacecraft and the exhaust plume.

Standard interferometry techniques have been used to measure electron and neutral densities in the exhaust plumes of Pulsed Plasma Thrusters (PPTs). Previous research used a single-color, heterodyne quadrature interferometer to acquire electron density measurements on "standard" PPT with a 20-J discharge across a 2.54-cm^2 square propellant face.[2] In addition to characterizing the plasma distribution, these measurements indicated the presence of a significant neutral population. Further measurements used a two-color interferometer to simultaneously measure both neutral and electron density near the propellant face to characterize the ablation controlled arc structure of the PPT.[3] In spite of the demonstrated capability, it became clear that conventional interferometry techniques had critical limitations when used on PPTs. First, the resolution was insufficient to quantify the neutral density at the thruster exit plane. Second, some PPT research and development shifted to the "microthruster" class with a

circular propellant face less than 7 mm in diameter.[4] Conventional interferometer configurations were incapable of transmitting the multiple laser passes needed to make a quantitative density measurement through the small scale length plasma.

To overcome the limitations of standard interferometers when used to characterize PPT plasmas, the apparatus is augmented with a Herriott Cell. A Herriott Cell consists of two highly-reflective concave mirrors facing each other in which laser light can be reflected a large number of times within the cavity. The number of reflections and the pattern of the laser passes within the cell are determined by the mirror curvature, separation, and entrance angles. The Herriott Cell holds two primary advantages over a single-pass interferometer. First, it increases sensitivity to plasma-induced phase shifts almost linearly with the number of reflections in the cell. Second, over long timeframes ($t > 50$ μs) the Herriott Cell increases the signal of the neutral density phase shift relative to the noise of the phase shift due to room vibrations. In addition, although the instrument has a fundamental decrease in spatial resolution compared to the single-pass interferometer, the beam geometries created by the Herriott Cell can be advantageous in selected applications.

The Herriott Cell can create beam patterns through the plasma which approximately fill a volume, a plane, or a point. The volume measurement can be valuable in measuring total specie inventory within the plasma. The planar measurement can be valuable for measuring the time-dependent plasma density crossing the exit plane of a plasma thruster. The point measurement is useful for performing measurements in small scale-length plasmas.

The Herriott Cell has been used for a variety of functions since its inception by D. Herriott for use as a laser resonator.[5] J. Altmann et al. first proposed its use in gaseous absorption measurements[6] and it has been used extensively for that purpose. In addition, Herriott Cells have been used for measurements of high reflectivity,[7] as an optical delay line,[8] and to produce a sequence of variable pulse separation light pulses.[9] The current effort is the first use in an interferometry application, where it is critical to maintain sufficient phase-front quality for interference after a large number of reflections.

This paper is directed towards validating the use of the Herriott Cell in interferometry applications. Analysis and experimental data are restricted to the planar configuration; however the conclusion regarding the usefulness of the device is applicable to the volume and point configurations. Section 2 describes the apparatus. Ray tracing analysis is used to illustrate planar beam geometries enabled by the Herriott Cell. In Section 3, analysis is used to show that phase front degradation and loss of scene beam intensity, concomitant with the large number of reflections from the Herriott Cell mirrors, does not introduce a systematic measurement uncertainty. In Section 4, the diagnostic capability is demonstrated with measurements of the electron and neutral densities in the plasma exhaust from electric propulsion thrusters.

2. Apparatus

2.1 Herriott Cell Interferometer

A schematic of the diagnostic layout is shown in Fig. 1. The lasers, acousto-optic modulator, optics, and detectors are positioned on an air-leveled optics table isolated

from the vacuum chamber. The Herriott Cell and plasma source are positioned on a second optics table within the vacuum chamber. The long-term drift of the optical path length on external optics table is ±3°. After a few milliseconds, relative drift between the optic tables is much greater than the laser wavelength.

The interferometer shown in Fig. 1 uses an Ar^+ laser at 488 nm with 150 mW output power. The laser is split into a scene and a frequency-shifted reference beam using a Bragg Cell acousto-optic modulator operating at 40 MHz. The scene beam enters and exits the vacuum chamber through a quartz view port. Mirror M5 in the reference beam path facilitates adjustment of the reference path length. As passes are added within the Herriott Cell, increasing the scene beam path length, this mirror is translated to equalize the two path lengths within the 10 cm coherence length of the laser. Detection of the recombined beam is accomplished with a photodiode biased in avalanche mode, amplified, and demodulated in quadrature using standard heterodyne detection techniques.[2,10]

The Herriott Cell, within the vacuum chamber, consists of two concave mirrors facing each other in which laser light can be reflected a large number of times within the cavity. One of the mirrors has an off-axis admission aperture that allows entrance of the beam within the diameter of the mirrors themselves. For configurations used in this work, the beam leaves the cell through the same aperture. The number of reflections is determined by the mirror separation and entrance angles. In the general three-dimensional configuration, the beam enters the cell at an angle offset both vertically and horizontally from the mirror centerlines and the reflection points trace an ellipse on the surface of

each mirror.[5,6,7] By eliminating one of the entrance angles, the passes can be confined to a single plane, ideal for measuring plasma density passing the exit plane of rocket nozzles. By separating the Herriott Cell mirrors to approximately twice the focal length, and focusing the input laser onto the Herriott Cell midpoint, the beams will converge near a single point,[5,6,7] which is useful for multi-pass measurements in small volumes. Only the planar configuration will be considered in detail within this paper.

2.2 Ray Tracing Analysis

To simplify integration with the interferometer, the planar configuration is generated in a retro-reflecting mode where the input and output beams are collinear. In practice, a slight angular offset is introduced between the input and output beams so that a mirror (M4 in Fig. 1) can be used to pick off the output scene beam and direct it towards the detector. The beams could be left collinear and a beamsplitter could be used instead of M4 in Fig. 1, however this decreases intensity at the detector by a factor of 4.

Planar retro-reflecting patterns are generated by arranging the Herriott Cell mirrors with collinear optic axis. The scene beam is input parallel to the optic axis, but spatially offset. Specific patterns are identified through ray-tracing analysis.[11] Figure 2 shows four examples of planar retro-reflecting patterns for a Herriott Cell with 50 mm diameter mirrors of 101 mm focal length. The input mirror has a 5 mm hole, 11 mm from the optic axis, through which the scene passes. Fig. 2a shows a six pass case where the mirrors are separated by 140 mm. Note that each line in Fig. 2 corresponds to two oppositely-directed rays. Figs. 2b, 2c, and 2d show the patterns for 10, 14 and 18 passes respectively. As shown in the figure, passes are added simply by increasing the

separation between the mirrors. The circle superimposed on the beam patterns in Fig. 2 is 4.4-cm in diameter, representative of the exit plane area of a standard PPT.[12]

3. Theory

The scene beam will experience a phase shift due to plasma electrons, neutrals, and vibrations which change the physical path length between optical components. The total phase shift can be written as (MKS units, radians).[2]

$$\Delta\phi = 2.8\times10^{-15}\lambda\int n_e dl - \frac{3.9\times10^{-29}}{\lambda}\int n_n dl + \frac{2\pi\Delta L}{\lambda} \quad (1)$$

where λ is the laser wavelength, n_e is the electron density, n_n is the neutral density, l is the path length through the plasma, and ΔL is variations in the total optical path length due to influences such as room vibrations and thermal drift. Equation 1 is converted to common density units by assuming that the path length through the plasma is equal to the size of the thruster exit plane multiplied by the number of laser passes. The measurement is then a line-averaged density across the exit plane of the thruster. Performing the line integration allows equation (1) to be rewritten as

$$\Delta\phi = (2.8\times10^{-15}\lambda Nl)n_e - (\frac{3.9\times10^{-29}Nl}{\lambda})n_n + (\frac{2\pi}{\lambda})\Delta L \quad (2)$$

where N is the number of reflections in the Herriott Cell.

The phase shift due to electron density can be separated from that due to neutrals and vibrations using a two-color interferometer, since the first term has a linear dependence on λ compared to the inverse dependence for the second and third terms.[13] The phase shift due to neutral density is separated from that due to vibrations through the use of the Herriott Cell. The mechanical vibrations are dominated by relative motion between the external and internal optics tables shown in Fig. 1. Adding passes within the Herriott Cell causes a negligible increase in ΔL. Therefore, adding reflections within the Herriott Cell increases the signal (phase shift due to neutrals and electrons) but does not significantly increase the noise (phase shift due to path length changes), resulting in an increased resolution for the device.

3.1 Phase Front Analysis

The main technical challenge in using the Herriott Cell for interferometric measurements is maintaining sufficient phase front quality to enable interference between the recombined beams after the large number of reflections within the cell. The quality of the phase front is decreased during every interaction with an optical element. Even with high surface-quality mirrors in the Herriott cell, increasing the number of reflections will eventually distort the phase-front by full wavelengths across the beam diameter.

These effects can be examined analytically. At the detector, the electric field for the scene and reference beams can be written as

$$E_{scene} = E_s e^{i(\omega_A t + \phi(t) + \gamma(x,y))} \quad (3)$$

$$E_{reference} = E_R e^{i(\omega+\omega_A)t} \qquad (4)$$

where ω is the laser frequency, ω_A is the acoustic frequency of the Bragg cell, Φ is the phase shift due to plasma and neutral density, and $\gamma(x,y)$ represents a phase distortion across the beam diameter. The total electric field at the detector is the sum of these components. The output voltage of the detector is proportional to the intensity, which can be calculated from the electric fields as

$$V \propto I = \frac{1}{2} EE^* \qquad (5)$$

where E and E^* are the electric field and its complex conjugate respectively. After some algebraic manipulation this reduces to

$$V\left(\frac{E_S}{E_R}\right) \propto E_R^2 \left[1 + \left(\frac{E_S}{E_R}\right)^2 + 2\left(\frac{E_S}{E_R}\right)\cos\left(\omega_A - \phi(t) - \gamma(x,y)\right)\right] \qquad (6)$$

For $E_R = E_S$ and perfect phase front ($\gamma(x,y)=0$), this reduces to the familiar expression

$$V \propto 1 + \cos(w_A t + \phi(t)) \qquad (7)$$

The detection electronics, in the ideal case of Eq. 7, then outputs voltages proportional to the sine and cosine of the phase shift $\varphi(t)$.

The effect of phase front distortion is examined using Eq. 6 and assuming that the two beam intensities are equal. Functional forms for the $\gamma(x,y)$ term are input, and the resultant voltage is calculated by integrating over the spatial extent of the recombined beam. A simple case of this analysis is illustrated in Fig. 3 where the 40 MHz waveform of Eq. 6 is calculated for various levels of phase-front distortion. The distortion here is assumed to be linear and only occur in one direction. The local intensities are integrated over a square cross-section indicative of the square active area of the photodetector. As the magnitude of the phase-front distortion increases, the intensity decreases, although the 40 MHz frequency remains. For 360-degree linear distortion, the 40 MHz signal disappears as expected. For distortion greater than a full wavelength, the 40 MHz signal reappears but with significant loss of intensity. Therefore significant phase-front distortion can be tolerated and still retain the 40 MHz acousto-optic frequency in the recombined beams. For curved phase fronts, similar effects are observed except that, (1) the 40 MHz signal can shift in phase as the phase-front distortion increases, and (2) at 360 degree average phase distortion, the 40 MHz signal may remain depending on the functional form assumed for the curvature.

The more critical issue is whether the phase-front distortion affects the apparent phase change that occurs when the plasma is introduced. This is examined in Fig. 4 where two signals, one with no distortion and one with a distortion of 135 degrees, are each assumed to have a 60 degree plasma phase shift. Although the signal intensity is reduced, in the case with significant phase-front distortion the full 60 degree plasma shift is observed in the 40 MHz waveform at the detector. This indicates, for the linear distortion case, that the amount of phase shift caused by the plasma density is not changed through the

process of integrating the intensity over the laser beam diameter of varying phases. Linear phase distortions do not cause systematic errors in the measurement of the plasma density. Analysis with curved phase fronts shows that an effective phase shift can be created between the undistorted and distorted case. However, the relative phase shift for the distorted case between the plasma and no-plasma case is still 60 degrees. The possible systematic error introduced by the phase front distortion cancels out and the measured phase shift is equal to that due to the plasma density. This indicates that phase front distortion introduces negligible systematic errors into the measurement.

The high number of surface reflections will also significantly decrease the scene beam intensity. Decreased intensity can be somewhat avoided by attenuating the intensity of the reference beam, or by adjusting the alignment or drive oscillation power of the acousto-optic modulator to increase the relative intensity of the scene beam. In practice, attenuating the reference beam by adding neutral density filters can also increase phase-front distortion. Adjusting the Bragg cell is limited to a small range in intensity variation.

Figure 5 shows Eq. 6 plotted for several relative intensities of the scene and reference beams. As expected from Eq. 7, the "50-50" curve (equal intensity) shows a simple 40 MHz oscillation. As the intensity imbalance is increased, the 40 MHz signal remains, although its relative magnitude decreases. The signal also obtains a DC offset. This is equivalent to the loss of fringe contrast that occurs in the similar situation in two-dimensional interferometers (without heterodyning). Band-pass filters at the input of the demodulation circuit will eliminate the DC offset leaving the 40 MHz signal with no phase distortion, albeit with a lower intensity. The reduced intensity will decrease the

signal-to-noise ratio, increasing random measurement uncertainty but not introducing a more serious systematic uncertainty.

4. Experimental Results

Experiments are performed at vacuum with typical background pressures of ~30 μTorr. The plasma source for these experiments is the PPT. Detailed description of this source is given by Burton and Turchi.[1] In particular, the PPT used for planar density measurements with the Herriott Cell is the UIUC PPT-4, which is a coaxial, electrothermal PPT with an exit plane diameter of 4.4 cm.[12]

Figure 6 shows the electron density co-plotted with the thruster current. The disparity between the start of the discharge and the observed electron density is due to plasma formation in a capillary which is then expanded through a nozzle. There is a short delay while the plasma travels the length of the nozzle. The measurement uncertainty is dominated by vibrations during a single firing. This early in the pulse, the vibration contribution to the phase shift is small, resulting in the tiny uncertainty bars shown.

A measure of the Herriott Cell effect is shown in Figs. 7 and 8. In Fig. 7 the electron density is plotted 2 μs after the discharge initiation for increasing number of passes through the Herriott Cell. In Fig. 7 a single-color interferometer is used so an approximation is made that all phase shift is due to electron density or vibrations, and neutral density is ignored. This is a reasonable approximation for validating the Herriott Cell since the phase shift due to the neutral density during the discharge is significantly (~20 times) less than that due to the electron density.[3] The data shown in Fig. 7 is from

four separate PPT firings. Deviations in the density are due to poor discharge reproducibility inherent to the device. It is clear that using the Herriott Cell reduces the measurement uncertainty due to vibrations to well below that due to discharge irreproducibility. Figure 8 shows the neutral density, 200 μs after the discharge. In this case it is assumed that the phase shift is due to neutral density and vibration-induced changes in the optical path length. The electron density can be ignored since the discharge current has decayed to zero and there is no longer an external energy source to support the ionization process to create electrons. The measurement uncertainty is observed to decrease with added passes through the neutral vapor. In the case shown in Fig. 8, the measurement uncertainty does not reduce to the point of providing a definitive neutral measurement, but the trend and potential benefits of the multi-pass configuration are clear. Additionally, Figures 7 and 8 illustrate an important feature. The results hold constant in both cases as the number of cell reflections increase, at least to within the irreproducibility of the plasma source used. This demonstrates that there are no beam refraction effects that could cause the number of exposed beams to change during the pulse.

Fig. 9 shows the phase shift due to mechanical noise at 200 μs plotted against the number of passes. This is the vibrational uncertainty contribution as the number of reflections increases. The key point of this data is to show that after the additional optic of the Herriott Cell is added (the two pass method uses only one flat mirror), there is no increase in the optic path length due to vibrations as the number of passes is increased from 6 to 14 to 18 reflections in the cell. Instead the measurement uncertainty is observed to remain relatively constant near 20 degrees in support of the conjecture that

the dominant source of vibrations is between the internal and external optic table. Additional laser passes can be added within the Herriott Cell without increasing vibration-induced measurement uncertainty.

5. Conclusions

A high resolution interferometer is developed by augmenting a standard heterodyne quadrature interferometer with a Herriott Cell to create a large number of passes through the medium. A retro-reflecting planar pattern is found to be easily integrated with the interferometer optics. Other patterns, such as a point measurement, are attainable with the Herriott Cell but are not explored in this work. Analysis is used to show that neither phase front distortion nor loss of scene beam intensity will introduce a systematic error to the measurement. Demonstrating the instrument on the plasma exhaust of a Pulsed Plasma Thruster shows an increase in resolution almost linear with the number of laser passes within the Herriott Cell. For neutral density measurements, the signal level of the phase shift due to density increases almost linearly with the number of passes compared to the noise level of phase shift due to room vibrations. These results indicate that the addition of a Herriott Cell to a quadrature heterodyne interferometer is both feasible and beneficial for increasing instrument resolution to both electron and neutral densities.

6. Acknowledgements

This work is supported by the Air Force Office of Scientific Research under Dr. Mitat Birkan. The experiments were performed in the Electric Propulsion Laboratory at Edwards AFB under the Air Force Research Laboratory Propulsion Directorate.

Figure Captions

Figure 1: Experimental Setup.

Figure 2: Growth of the retro-reflecting beam pattern in the Herriott Cell.

Figure 3: Detector output signal for varying magnitudes of phase-front distortion.

Figure 4: Effect of phase-front distortion when a plasma-induced phase front is present.

Figure 5: Effect of non-balanced intensities on the interferometer signal at the detector.

Figure 6: Current pulse and electron density for PPT-4 with vertical vibrational error bars due to 18 passes in Herriott Cell.

Figure 7: Electron density uncertainty at 2 μs decreases with increasing passes.

Figure 8: Neutral density uncertainty at 200 μs after discharge decreases with increasing passes.

Figure 9: Mechanical noise at 200 μs after trigger is constant with increasing passes.

References

[1] R. L. Burton, P. J. Turchi, "Pulsed Plasma Thruster," *Journal of Propulsion and Power*, Vol. 14, No. 5, 1998, pp. 716-735.

[2] G. G. Spanjers, K. A. McFall, F. S. Gulczinski, R. A. Spores, "Investigation of Propellant Inefficiencies in a Pulsed Plasma Thruster," AIAA Paper No. 96-2723, July 1996. Note in Reference 1 that the units on Eq. 3 are erroneously stated as MKS-degrees. The units should be MKS-radians.

[3] E. L. Antonsen, R. L. Burton, G. G. Spanjers, "High Resolution Laser Diagnostics in Millimeter-Scale Micro Pulsed Plasma Thrusters," IEPC Paper 01-157, July, 2001.

[4] Spanjers, G.G., Bromaghim, D.R., Lake, Capt. J., Dulligan, M., White, D., Schilling, J.H., Bushman, S.S., Antonsen, E.L., Burton, R.L., Keidar, M., Boyd, I.D., "AFRL MicroPPT Development for Small Spacecraft Propulsion," 38th AIAA/ASME/SAE/ASEE Joint Propulsion Conference, AIAA Paper No. 2002-3974, Indianapolis, IN, July 2002.

[5] D. R. Herriott, H. Kogelnik, R. Kompfner, "Off- Axis Paths in Spherical Mirror Interferometers," Applied Optics 3, 1964, 523.

[6] J. Altmann, P. Pokrowsky, "Sulfur Dioxide Absorption at DF Laser Wavelengths," Applied Optics Vol. 19, No. 20, 1980, pp. 3449-3452.

[7] D. R. Herriott, H. J. Schulte, "Folded Optical Delay Lines," Applied Optics Vol. 4, No. 8, 1965, pp. 883-889.

[8] J. Brochard, P. Cahuzac, "Use of Multi-Path Optical Cavities in some Saturated Absorption Experiments. Frequency Scale and Optical Delay Line." J. Optics (Paris) Vol. 8, No. 3, 1977, pp. 207-211.

[9] J. Altmann, R. Baumgart, C. Weitkamp, "Two Mirror Multipass Absorption Cell," Applied Optics Vol. 20, No. 6, 1981, pp. 995-999.

[10] A. R. Jacobsen, Rev. Sci. Instrum. 49, p. 673 (1978).

[11] Stellar Software, Berkeley, CA, www.stellarsoftware.com

[12] S. S. Bushman, R. L. Burton, "Heating and Plasma Properties in a Coaxial Gasdynamic Pulsed Plasma Thruster," Journal of Propulsion and Power, Vol. 17, No. 5, pp. 959-966, 2001.

[13] E. L. Antonsen, *Herriott Cell Interferometry for Pulsed Plasma Density Measurements*, MS Thesis, University of Illinois U-C, 2001.

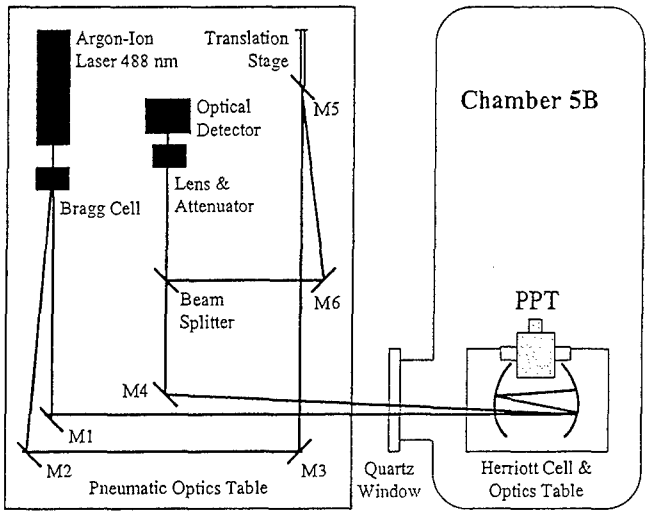

Figure 1. Antonsen *et al.*, RSI, "Herriott Cell Augmentation..."

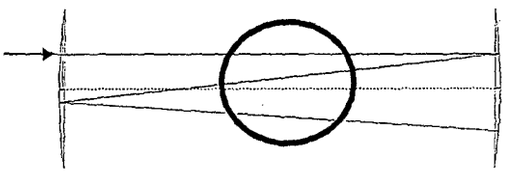

a.) 6 Pass, 140 mm Separation

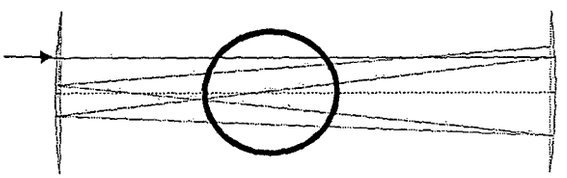

b.) 10 Pass, 168 mm Separation

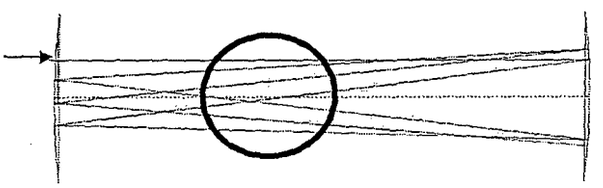

c.) 14 Pass, 179 mm Separation

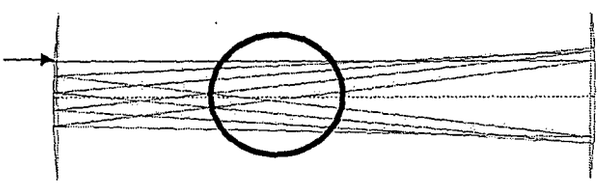

d.) 18 Pass, 184 mm Separation

Figure 2. Antonsen *et al.*, RSI, "Herriott Cell Augmentation..."

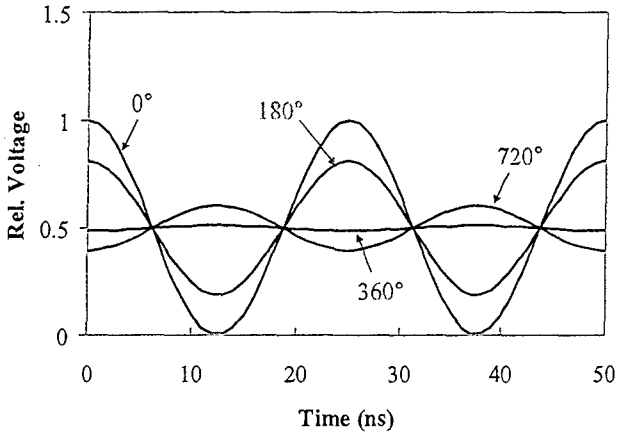

Figure 3. Antonsen *et al.*, RSI, "Herriott Cell Augmentation..."

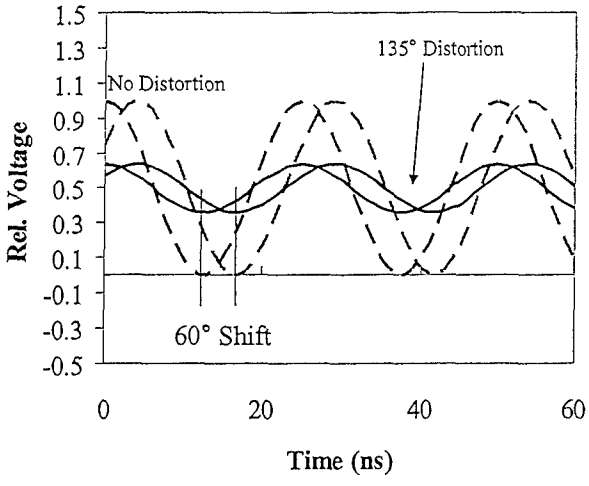

Figure 4. Antonsen *et al.*, RSI, "Herriott Cell Augmentation..."

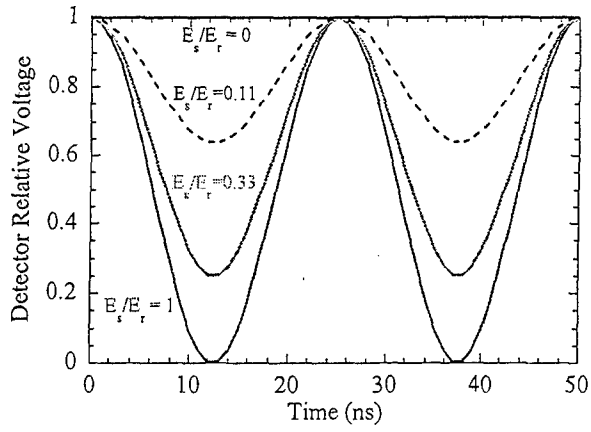

Figure 5. Antonsen *et al.*, RSI, "Herriott Cell Augmentation…"

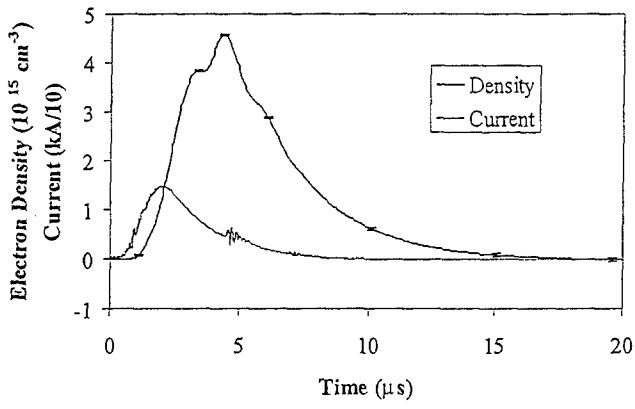

Figure 6. Antonsen *et al.*, RSI, "Herriott Cell Augmentation..."

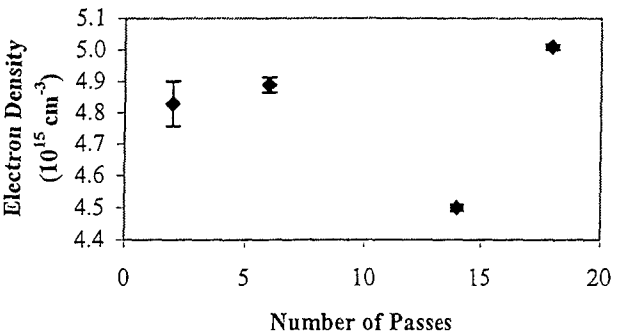

Figure 7. Antonsen *et al.*, RSI, "Herriott Cell Augmentation..."

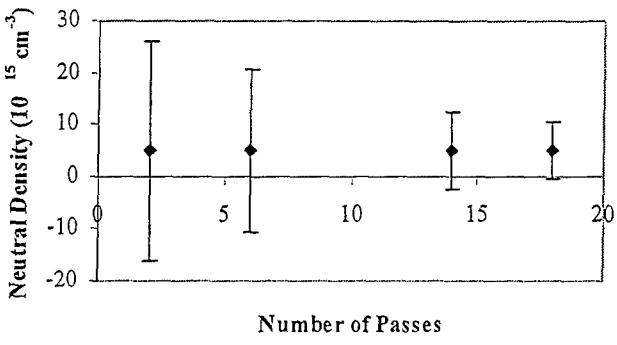

Figure 8. Antonsen *et al.*, RSI, "Herriott Cell Augmentation..."

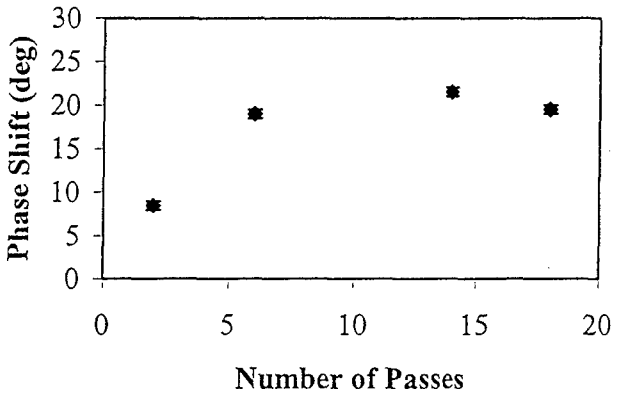

Figure 9. Antonsen *et al.*, RSI, "Herriott Cell Augmentation..."